

k-strip: A novel segmentation algorithm in k-space for the application of skull stripping

Moritz Rempe^{1,2}, Florian Mentzel², Kelsey L. Pomykala¹, Johannes Haubold¹,
Felix Nensa¹, Kevin Kröninger², Jan Egger^{1,3,4,5}, Jens Kleesiek^{1,5,6}

Abstract—Objectives: Present a novel deep learning-based skull stripping algorithm for magnetic resonance imaging (MRI) that works directly in the information rich k-space.

Materials and Methods: Using two datasets from different institutions with a total of 36,900 MRI slices, we trained a deep learning-based model to work directly with the complex raw k-space data. Skull stripping performed by HD-BET (Brain Extraction Tool) in the image domain were used as the ground truth.

Results: Both datasets were very similar to the ground truth (DICE scores of 92%-98% and Hausdorff distances of under 5.5 mm). Results on slices above the eye-region reach DICE scores of up to 99%, while the accuracy drops in regions around the eyes and below, with partially blurred output. The output of k-strip often smoothed edges at the demarcation to the skull. Binary masks are created with an appropriate threshold.

Conclusion: With this proof-of-concept study, we were able to show the feasibility of working in the k-space frequency domain, preserving phase information, with consistent results. Future research should be dedicated to discovering additional ways the k-space can be used for innovative image analysis and further workflows.

Index Terms—Magnetic resonance imaging (MRI), Brain extraction, Skull stripping, k-space, Frequency domain, Deep learning, Complex convolutional networks.

I. INTRODUCTION

Image scanners provide more data of patients, than can actually be manually reviewed and fully annotated in the current time-limited clinical routine. For example tumor size is often measured by maximum 2D tumor diameter, rather than a more complete tumor volume [1, 2]. Hence, there is a strong desire for automated or at least semi-automated methods, helping to process medical images, or medical information in general [3].

An important example is skull-stripping or brain extraction, the process by which the skull and non-brain tissues are removed from magnetic resonance images (MRI) [4, 5, 6]. Skull stripping is a fundamental step in neuroimage pre-processing because the accuracy of subsequent image processing, such

as registration [7] or tumor segmentation [9, 8], relies on the accuracy of the skull-stripping. Not only is the process important for accuracy of further pipelines, but it is also an important step in anonymization [10]. Furthermore, the extracted skull information can be important for cranial implant design [11]. Unfortunately, manual removal of non-brain tissues is a complex laborious process [12], that often results in inter- and intra-rater incongruities affecting reproducibility in large scale studies [6]. However, in recent years due to theoretical advances in the field and a rise in availability of inexpensive computing power, many deep learning-based automatic skull stripping methods have been proposed [6, 12, 13, 14].

Automatic skull stripping is an important, more precise, time saving technique, but looking even further, imagine the exploration of tactics for overcoming the limits in human vision. Medical images are much richer in information than what the human eye can discern [15], and a lot of this untapped data is in the k-space, or the matrix of raw MRI data [16]. Quantitative imaging features, also called “radiomic features,” can provide fuller information about intensity, shape, texture, size and volume [15, 17]. To our knowledge, the k-space has not yet been utilized for deep learning-based segmentation. In this proof-of-concept work, we show that skull stripping is already possible in the k-space, and reconstruction of the k-space results, leads to a stripped skull in the image space.

A. Previous work

The “gold standard” for brain extraction and tissue annotation is still a manual segmentation. But because of its high time effort and the problem of inter- and intraindividual variance, leading to non-reproducible results, there has been an urgent search for methods to automate this task [18]. The currently available techniques for brain extraction can be subdivided into five groups [19]:

- mathematical morphology-based methods,
- intensity-based methods,
- deformable surface-based methods,
- atlas-based methods,
- and hybrid methods.

Morphology-based methods, like by Brummer et al. [20], use thresholds and edge-detection algorithms to distinguish between brain and non-brain tissue. The output quality depends on morphological parameters, which have to be set beforehand. Intensity-based methods extract brain tissue by solely using

¹Institute for AI in Medicine (IKIM), University Hospital Essen, Girardetstraße 2, 45131 Essen, Germany.

²Department of Physics of the Technical University Dortmund, Otto-Hahn-Straße 4a, 44227 Dortmund, Germany.

³Computer Algorithms for Medicine Laboratory, 8010 Graz, Austria.

⁴Institute of Computer Graphics and Vision, Graz University of Technology, Inffeldgasse 16, 8010 Graz, Austria.

⁵Cancer Research Center Cologne Essen (CCCE), University Medicine Essen, Hufelandstraße 55, 45147 Essen, Germany.

⁶German Cancer Consortium (DKTK), Partner Site Essen, Hufelandstraße 55, 45147 Essen, Germany.

intensity-thresholds, based on the different intensities of brain and non-brain tissues [21], [22]. One drawback of this technique is that it is prone to anomalies like artifacts, pathologies or simply low resolution. Using curve evolution and energy functions, deformable surface-based methods perform a brain extraction by solving an optimization problem. A widely used tool applying deformable methods is *BET* (Brain Extraction Tool) by the *FMRIB Software Library* (FSL) [23]. Wang et al. [24] developed an algorithm that employs a predefined atlas to create a registration mask, followed by refinements. Another algorithm using prior information is *BEaST* by Eskildsen et al. [25], semi-automatically constructing a library of 80 prior shape masks beforehand. At last, hybrid methods combine multiple of the previous methods like the *Hybrid watershed algorithm* (HWA) [26], combining the watershed algorithm [27] with a deformable surface model [28].

Lately, with the advent of deep neural networks [29, 30], more and more algorithms have been published that use the benefits of machine learning, introducing another brain extraction method. Kleesiek et al. [31] introduced a 3D convolutional neural network (CNN), which is able to also work with pathological data, as most of the algorithms proposed before struggle when facing pathologies like tumorous tissue or abnormal anatomies. Another machine learning approach is *HD-BET* by Isensee et al. [32], which has the benefit of being trained on different sequences, like pre- and post-contrast T1, T2 and FLAIR. However, all these methods have one mayor property in common: They do the skull stripping in the image domain after a Fourier transformation has been performed.

Bassey et al. [33] published a survey about complex-valued neural networks (CVNN), giving an insight in different works that have been done with CVNNs. These networks can take complex valued data as input, which is of importance for this work. Another field of use for these kind of networks is Quantum Computing [34] by taking advantage of the representational capacity of complex valued numbers.

In the medical domain, deep learning approaches have mainly been used for interpolation and reconstruction on raw data. Recently, Han et al. [35] proposed an approach to interpolate missing k-space data for better reconstruction results by using a convolutional neural network and a low-rank Hankel matrix completion. Another approach for interpolating partial Fourier reconstructions was introduced by Huang et al. [36]. They use convolution in *k*-space to estimate missing phase information and recover the missing data via Hermitian operations. Huang et al. [37] combine the task of reconstruction and segmentation, creating an end-to-end framework, which uses raw data information in the reconstruction process and attention modules, possibly preserving important image features. *SARA-GAN* [38] is a reconstruction method based on a generative adversarial network (GAN) [39] with Self-Attention mechanisms and a relative average discriminator. The generator uses raw data to create more realistic reconstructions with a higher peak signal-to-noise ratio. Bresch et al. [40] proposed an algorithm, based on a gradient descent procedure, for unsupervised edge detection of vocal tracts in the MRI

frequency domain. A 2-D Fourier transform of a polygonal shape function is used to compute contour parameters by optimizing an overdetermined nonlinear least squares problem.

By performing post processing in the image space, one does not only risk to work on data which has lost information after transformation, but also neglects half of the available data - the phase information. In this work, however, a novel network is proposed, which performs skull stripping in the frequency domain, the k-space. *K-strip* is a network, based on U-Net [41], which can take complex data as input. By acting as a proof-of-concept, the goal of this publication is to show the feasibility of working on raw data, possibly preserving valuable information. In the following, we will explain basic concepts for understanding the raw data domain of MRI. Then we elaborate on the dataset and network architecture. Finally, the results are presented and discussed.

II. MATHEMATICAL BACKGROUND

A. Fourier Transformation

A Fourier transformation [42] converts a 2D-signal from the time-domain into the frequency-domain or from the spatial-domain into the spatial-frequency-domain by applying Eq. 1.

$$S(k_x, k_y) = \int_x \int_y s(x, y) \exp(-i2\pi k_x x) \exp(-i2\pi k_y y) dx dy \quad (1)$$

The inverse form (inverse Fourier transformation) of this equation is used to transform the raw MRI data into image space. No information is lost during this process. In signal processing, an efficient algorithm, called *Fast Fourier Transformation* (FFT) [43] is used for transforming between the two domains. There have been some implementations of neural networks using the Fourier domain to speed up training. Mathieu et al. [44] transform the input and the convolution kernel of a CNN into the Fourier domain. Convolutions in the spatial domain are equivalent to pointwise multiplications in the frequency domain. That way, by applying the FFT on the input data, the computational complexity and time can be reduced due to less operations. In this regard, Pratt et al. [45] were able to reduce computation time for large images in CNNs by applying Fourier pooling and convolution.

B. *k*-space

The *k*-space, or the frequency domain, is the raw data domain of MRI images. By applying a Fourier transformation, k-space data can be transformed into the image space [46]. By applying different gradients during an MRI scan, the protons resonances are encoded with both frequency and phase. Eq. 2 depicts the way the k-space is filled, with *m* and *n* being the number of data points acquired and γ the gyrosopic moment:

$$k_x = m\gamma G_x \Delta T \quad , \quad k_y = n\gamma \Delta G_y T_y \quad (2)$$

While the frequency-encoding gradient G_x is applied over varying time periods ΔT to fill the k-space in the x -direction, the phase-encoding gradient G_y is varied in strength during a fixed time period T_y to fill in the y -direction. Data points in the center of the k-space correspond to low frequencies, reflecting textures in image space. In the periphery, data points are encoding high frequencies, translating into edges and boundaries in image space. Data in image space can also be transformed back into the frequency domain by applying an inverse Fourier transformation. Data points in the frequency domain are complex valued, containing information about the phase and magnitude.

The image, on which skull stripping is performed, consists of the transformed magnitude data. Raw data in MRI does not only consist of magnitude, but also phase information. This information can be used in differentiating tissue types, which do not differ in magnitude. Phase information can also be used for flow detection [47, 48]. A more detailed look into k-space and other aspects of magnetic resonance imaging can be found in [49].

Due to sparseness of available raw data, in this work already transformed data has been inverse Fourier transformed to create artificial k-space data. The network was trained on different data sets, containing healthy and pathological scans.

III. MATERIALS AND METHODS

A. Dataset

Two datasets are used in this work, one provided from the University Hospital Essen, consisting of 30 000 T_1 brain MRI 2D-slices from 207 patients in image space (IRB 21-10487-BO). Some of the scans contain pathologies like glioblastomas multiforme (GBM) [50], giving the possibility to prove the feasibility of working with pathological data in k-space. The slices are all preprocessed by padding them into the shape 512×512 pixels. The dataset also comes with a ground truth in form of skull stripped scans, performed with HD-BET [32]. The other dataset is obtained from the NYU fastMRI Initiative database (fastmri.med.nyu.edu) [51, 52], containing 6900 fully sampled brain MRI scans. For anonymization, the FastMRI dataset does not include slices from the eyes downwards. The ground truth is again created via HD-BET. It was noticed, that HD-BET is not extracting the brain tissue as reliable as with the other dataset, cutting out parts in the middle of the brain in 8% of the scans. For training and testing on the FastMRI dataset, only one slice of the middle part of the brain is used for each individual scan. The slices are transformed into k-space via the PyTorch Fast Fourier Transformation function `torch.fft` [53]. This artificial k-space data does not contain the original phase information, but we are convinced, that non-artificial data will produce even better results, while preserving phase information. Before passing the complex k-space data into the network, it is mapped into the range $[0, 1]$ by standardizing the real and imaginary values separately and concatenating them back together again afterwards. The data is also augmented by randomly flipping them vertically and rotating them in the range of $[-10^\circ, 10^\circ]$. Augmentation

is performed in image space and then transformed into the k-space. We use a train-test-split with the ration of 80-20 commonly used in other works.

B. Network Architecture

K-strip is a complex valued convolutional neural network consisting, like U-Net, of a down-sampling path and an up-sampling path. The architecture of k-strip is shown in Fig. 1. In the down-sampling path (left side of Fig. 1), the input is split into multiple feature channels and is down-sampled via pooling. With increasing network depth, learned features are becoming more and more specific, while also increasing the computational complexity. By pooling after each convolution layer, this complexity is reduced to speed up the computation time and reduce the memory usage. The initial 2D-input size is $1 \times 512 \times 512$ (number of channels \times height \times width) and is abstracted into feature maps via four complex double convolutions to the size of $1024 \times 32 \times 32$. The input is then up-sampled again, until it reaches its initial size.

The concept of complex convolution layer is the same as of normal convolution layers, with the difference, that instead of a simple convolution, we now work with a complex convolution matrix W , which acts as the kernel of size 3×3 and performs a complex convolution (Eq. 3), as seen in [54]:

Complex convolution matrix:

$$W = X + iY$$

Complex data:

$$d = a + ib \quad (3)$$

Complex convolution:

$$W * d = (X * a - Y * b) + i(X * b - Y * a)$$

Each *cConv*-block consists of two complex convolutions following a complex ReLU (cReLU) activation function and a complex Batch normalization. After each cConv-block, the number of features is doubled. *cReLU* applies a ReLU activation on the real and the imaginary part separately and combines the output back into a complex number:

$$\text{cReLU} = \text{ReLU}(\text{Re}\{d\}) + i\text{ReLU}(\text{Im}\{d\}). \quad (4)$$

By applying a complex batch normalization (Eq. 5, as seen in [55]) after each activation function, the output is normalized per batch, preventing unbalanced gradients within the network [56]:

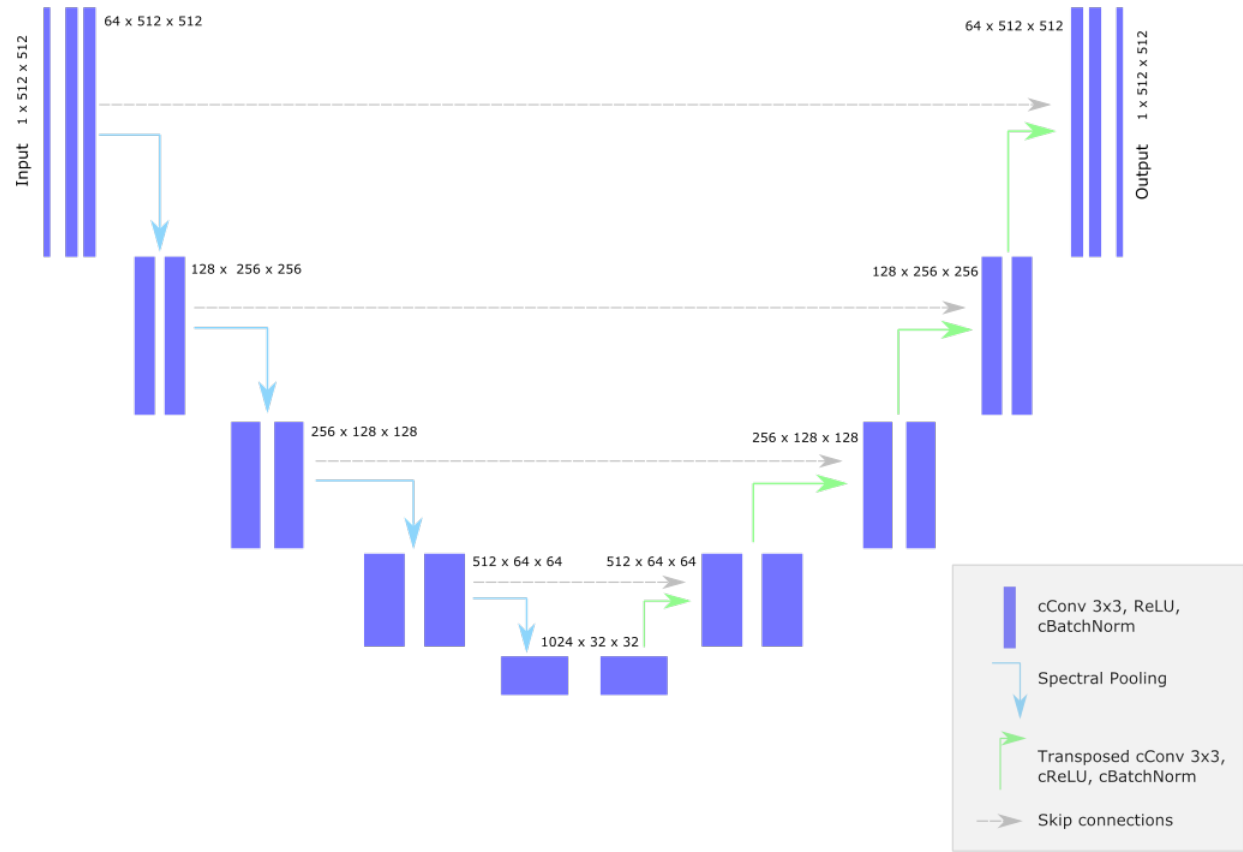


Fig. 1. Network architecture of k-strip, with a down-sampling path (left branch) and a up-sampling path (right branch). The blue boxes correspond to the convolutions and their feature maps. The numbers above these boxes depict the input numbers of channels, height and width.

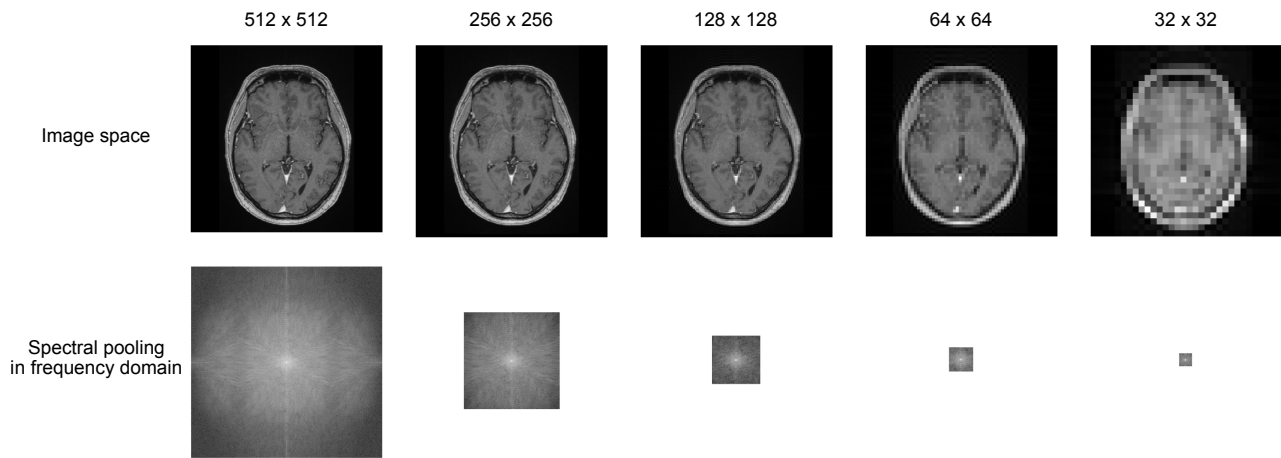


Fig. 2. Spectral pooling with a pooling kernel of size two. The k-space, pictured logarithmic and absolute valued, is halved with every pooling step, which leads to a decreasing resolution. Even after reducing the initial k-space by 95%, the object shape is still recognizable.

Complex Batch Normalization of x :

$$\tilde{x} = (V)^{-\frac{1}{2}}(x - E[x])$$

Covariance matrix:

$$\begin{aligned} V &= \begin{pmatrix} V_{rr} & V_{ri} \\ V_{ir} & V_{ii} \end{pmatrix} \\ &= \begin{pmatrix} \text{Cov}(Re\{x\}, Re\{x\}) & \text{Cov}(Re\{x\}, Im\{x\}) \\ \text{Cov}(Im\{x\}, Re\{x\}) & \text{Cov}(Im\{x\}, Im\{x\}) \end{pmatrix} \end{aligned} \quad (5)$$

Spectral pooling [57] reduces the image size, by cutting the periphery of the k-space by half its size in each layer. Even with cutting the high frequencies and thus reducing the input size by over 95%, the initial shape is still recognizable. By downsampling the input, the learned feature maps can focus on the most important structural elements, while reducing the computational complexity drastically. Spectral pooling on exemplary brain MRI images is shown in Fig. 2. Skip connections provide an additional path for the gradient by skipping some layers and feeding the output directly into the next layers. That way, the problem of vanishing gradients can be avoided, as even when some gradients approach zero, they are complemented by gradients of previous layers [58].

K-space is an overlap of many different frequencies together resulting in a final image. Because of this property, a traditional assignment into two classes, as done in image space, is not possible. Therefore, our network translates the input k-space into a k-space of a skull stripped scan by adjusting the frequency values according to the principle of *image-to-image* networks. To speed up computation and possibly enforcing better results, the desired output of the network, as well as the ground truth, are the skulls without brain tissue. The output can then be subtracted from the original input to receive a brain extracted image.

C. Training

For training, an Adam optimizer [59] with an initial learning rate of 1×10^{-4} is used. The network output is compared with the ground truth using the complex L1-loss, also known as least absolute errors (LAE). The ground truth consists of the skulls without brain tissue transformed into k-space. The skull data is calculated by subtracting the skull strips, created by HD-BET, from the original scan in image space. Training stops with the 100th epoch, because the validation loss does not further decrease at around this point. The overall training time takes two weeks on an *NVIDIA RTX A6000* GPU with 48GB of graphics memory.

D. Evaluation Metrics

For evaluation we decided to use two metrics, one being the Dice coefficient (DSC) [60] as an overlap measure between the brain segmentation X and the reference mask Y :

$$\text{DSC} = \frac{2|X \cap Y|}{|X| + |Y|} = \frac{2TP}{2TP + 2FP + 2FN}. \quad (6)$$

The Dice coefficient takes values in the range of $[0.0, 1.0]$, with 1.0 being a perfect segmentation, identical to the ground truth. The directed Hausdorff distance (DHD) [61] is used for evaluating maximum deviations, with a value starting at 0 mm for no deviations, increasing with wider outliers in the segmentation mask:

$$\text{DHD}(X, Y) = \max_{x \in X} \min_{y \in Y} \|x - y\|. \quad (7)$$

The results on the GBM set are also compared with the Brain Extraction Tool by the *FMRIB Software Library* (BET-FSL). To compare k-strip with methods working in the image domain, the output needs to be Fourier transformed, followed by creating a binary mask. Due to non-perfect image-to-image translations, the output contains some frequencies, which result in shadows around the skull stripped image. That is the reason for creating the binary mask, a threshold is used to classify the two classes (brain and non-brain tissue). After quantitative evaluations, the threshold is set to the mean value of the image domain data. All values below threshold are set to zero.

Additionally, scans with ground truth masks containing less than 20 000 pixels unequal zero are discarded, because these scans only include the most superior part of the brain or no brain tissue at all. The corresponding ground truth masks are often false or incomplete. Aside from that, k-strip does not produce images with all pixel being zero, when no brain tissue is existent, rather producing an image containing only faint background noise.

IV. RESULTS

Fig. 3 and 4 show some results of different slices in the GBM test dataset. On the left side is the input in image space and in k-space (the k-space data being fed into the network). The pictured k-space is logarithmic and absolute valued, as the center has values of magnitudes larger than the periphery and the k-space is complex valued. The networks prediction is transformed into image space (top) and then via threshold transformed into a binary mask (bottom). On the right side is the difference of the ground truth and prediction of image space and binary mask, respectively.

The corresponding DSC and HD in dependence of HD-BET and BET-FSL are displayed in Tab. I. Listed are the scores for the best prediction, the worst prediction and the average scores on the test set.

Brain extraction in the region above the eyes (as in Fig. 3) works very well with DSCs above 95%. The accuracy drops in regions around the eyes and below, with partially blurred output. Poor skull stripping, as in Fig. 4 may also occur because of threshold problems leading to erroneous binary masks, as well as mirroring artifacts.

Fig. 5 shows one result on the FastMRI test dataset, Tab. II the corresponding scores. The target brain extraction made by

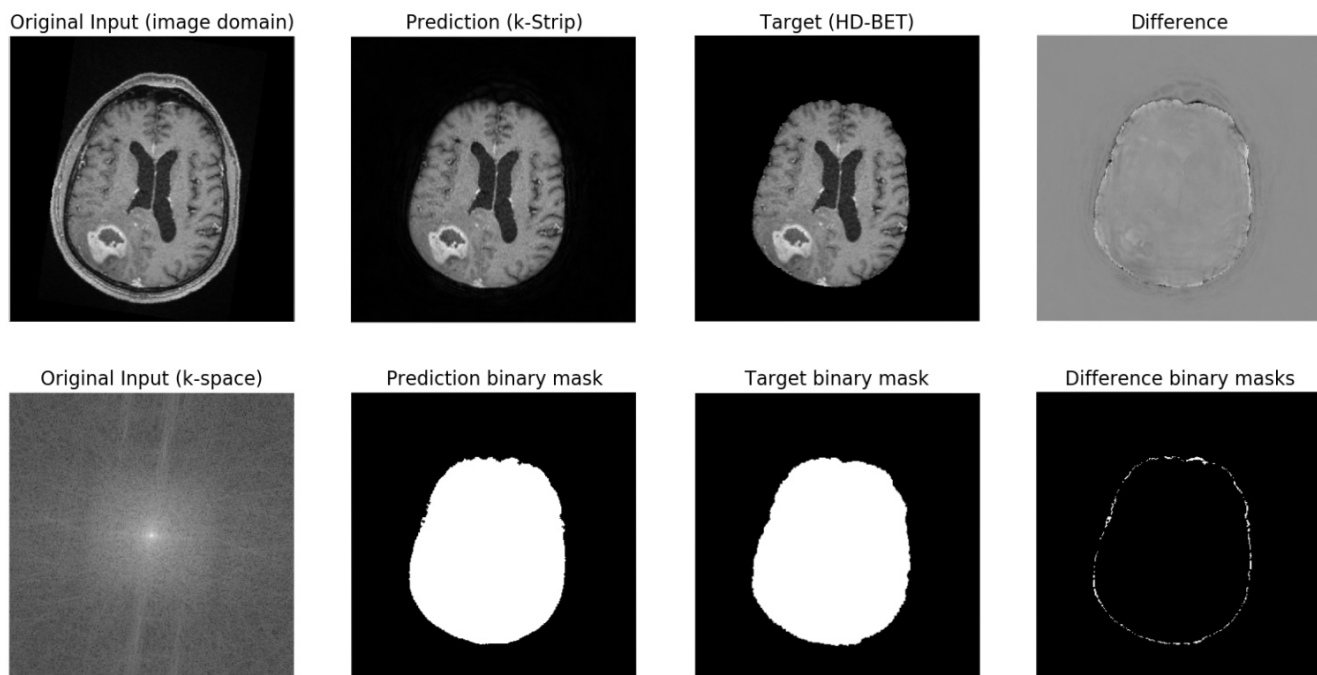


Fig. 3. Output example from the glioblastoma multiforme (GBM) test set for the brain region above the eyes: On the left side is the input in image space and in (for illustration) absolute valued logarithmic k-space (the k-space data being fed into the network). The networks prediction is transformed into image space (top) and then via threshold transformed into a binary mask (bottom). On the right side is the difference (ground truth - prediction) of image space and binary mask, respectively.

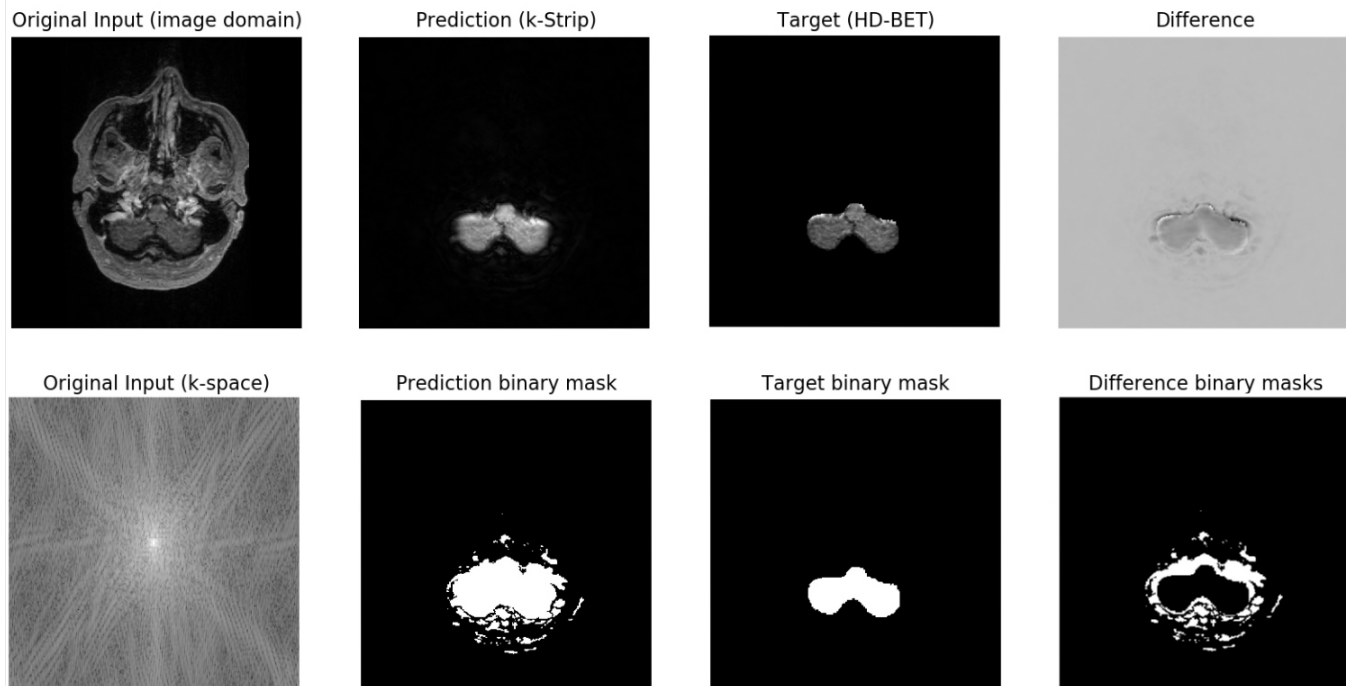


Fig. 4. Output example from the glioblastoma multiforme (GBM) test set from the brain region below the eyes: On the left side is the input in image space and in (for illustration) absolute valued logarithmic k-space (the k-space data being fed into the network). The networks prediction is transformed into image space (top) and then via threshold transformed into a binary mask (bottom). On the right side is the difference (ground truth - prediction) of image space and binary mask, respectively.

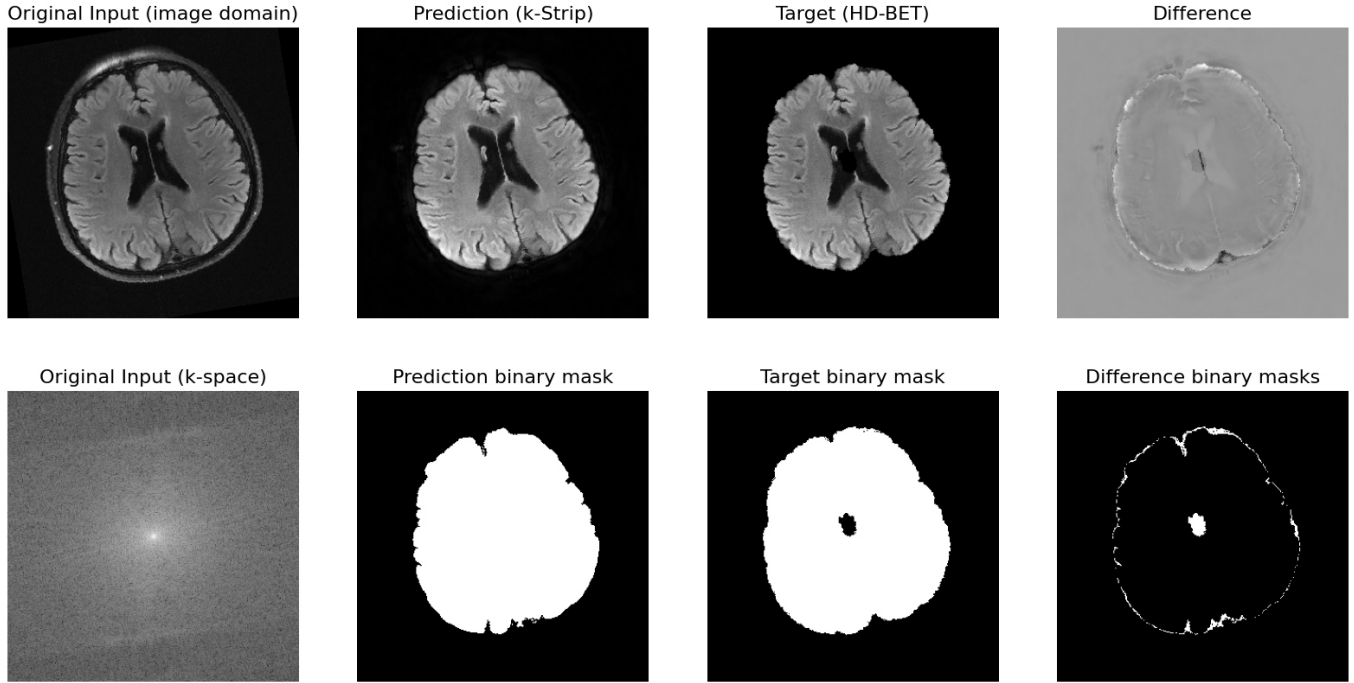


Fig. 5. Output example from the FastMRI test set: On the left side is the input in image space and in (for illustration) absolute valued logarithmic k-space (the k-space data being fed into the network). The networks prediction is transformed into image space (top) and then via threshold transformed into a binary mask (bottom). On the right side is the difference (ground truth - prediction) of image space and binary mask, respectively. K-strip performs better than HD-BET, as HD-BET cuts out parts inside the brain.

TABLE I

BEST, WORST AND AVERAGE RESULTS ON THE GLIOBLASTOMA MULTIFORME (GBM) TEST DATA, WITH HD-BET OUTPUT AS GROUND TRUTH AND BET-FSL AS ANOTHER SKULL STRIPPING TOOL.

	HD-BET		BET-FSL	
	DICE (%)	DHD (mm)	DICE (%)	DHD (mm)
Best	0.991	4.796	0.966	6.856
Worst	0.645	9.110	0.592	11.203
Overall	0.921	5.440	0.901	6.937

HD-BET shows the mentioned cut-outs in the middle of the brain tissue. This may be caused by the fact, that the scans do not contain the whole brain-anatomy. The presented k-strip algorithm does not produce these erroneous segmentations.

TABLE II

BEST, WORST AND AVERAGE RESULTS ON THE FASTMRI TEST DATA, WITH HD-BET OUTPUT AS GROUND TRUTH.

	DICE (%)	DHD (mm)
Best	0.983	4.243
Worst	0.964	5.099
Overall	0.981	4.405

V. DISCUSSION

In this paper, we proposed a novel framework based on the U-Net architecture for brain extraction in k-space, in which the raw data of MRI is recorded. This proof-of-concept study shows the feasibility of working in the frequency domain and, thus, preserving phase information, while achieving consistent results. While only being trained on T1 scans, we believe that the network will also perform well on other sequences, assuming the corresponding training data is provided.

In regions above the eyes, the predicted output almost matches the HD-BETs output, while differing sometimes in regions of the eyes and below. It has to be noted, that with the provided training data, k-strip can not outperform HD-BET, as its skull strips act as the ground truth.

The output of k-strip shows often smoothed edges at the demarcation to the skull, the reason being the nature of the k-space and the chosen approach. As we only change the values in k-space, k-strip is not able to make exact cuts in the image domain. This may change with more training data or further customization of the network. It is also noticeable, that in the prediction, the center of the k-space is much more similar to the ground truth, than the periphery, as can be seen in Fig. 6. With the center having values of magnitudes larger than the periphery, differences in the output are much more punished by the network (stronger weight-changes) than differences in the periphery. One approach for future work would be changing the loss function, taking into account these magnitudes with,

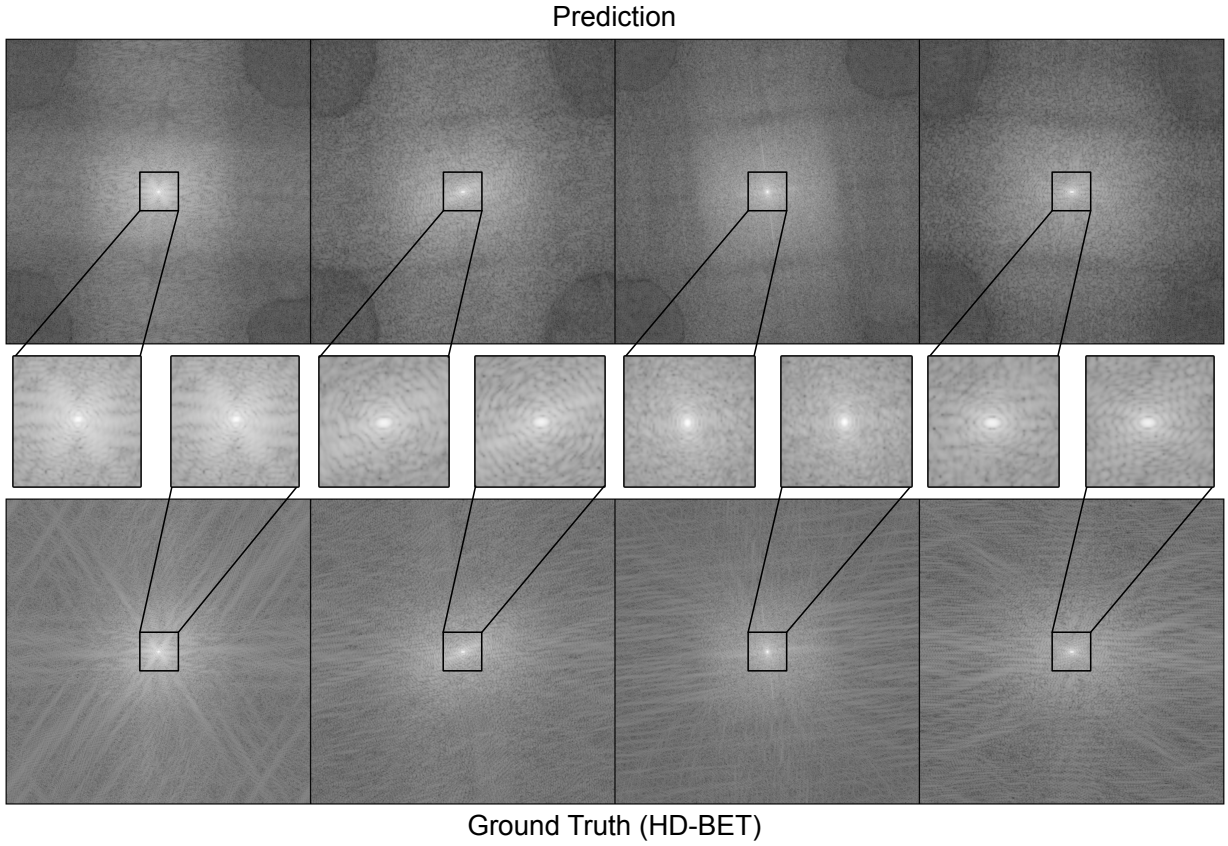


Fig. 6. Results on GBM test dataset in the k-space. Prediction of k-strip (top) and the corresponding ground truth by HD-BET (bottom), each with a cutout of the center of the k-space. The pictured k-space is logarithmic and absolute valued. While the wide periphery does not match the ground truth, the center of the predicted k-space resembles the one of the ground truth. K-strip seems to focus on the important information lying in the middle of k-space.

for example, a logarithmic part.

In regions below the eyes, our threshold method for creating binary masks, does not perform very well. But it does reveal mirroring artifacts, which do not matter in regions above the eyes, due to much better segmentation results. The network seems to faintly produce a mirrored segmentation besides the main segmentation, visible in Fig. 4, but this effect needs further examination. We also noticed, that HD-BET sometimes cuts out spots inside the brain, maybe due to unusual anomalies. K-strip does not seem to have problems with those cases, but does not produce as fine cuts as HD-BET does.

Reducing the size of the k-space input, using spectral pooling beforehand, would lead to faster training times, while preserving most of the details. A decision has to be made here whether the finest details provided by the k-space periphery are more important compared to faster training times, or vice versa.

In future work, we want to expand the concept to other segmentation tasks, like tumor segmentation, and work with real raw data, containing valuable phase information, as well as further optimization of the existing network.

VI. CONCLUSION

K-strip is a novel complex valued CNN, which enables brain extraction (segmentation) on raw data of MRI scans in the k-space. To the best of our knowledge, this is the first Deep Learning-based network doing skull stripping in the k-space of MRI data. Hence, this work acts as a proof-of-concept study, while achieving comparable results as HD-BET, a state-of-the-art network, working in the image space. We hope that in future, more works will investigate the possibilities and benefits of working in k-space, for example, preserving the "additional" phase information for tumor classification and tissue differentiation.

VII. ACKNOWLEDGEMENT

This work received funding from enFaced (FWF KLI 678), enFaced 2.0 (FWF KLI 1044) and KITE (Plattform für KI-Translation Essen) from the REACT-EU initiative (<https://kite.ikim.nrw/>).

REFERENCES

- [1] Jan Egger et al. "A medical software system for volumetric analysis of cerebral pathologies in magnetic resonance imaging (MRI) data". In: *Journal of medical systems* 36.4 (2012), pp. 2097–2109.

- [2] Markus Zimmermann et al. "CT-based whole-body tumor volumetry versus RECIST 1.1: Feasibility and implications for inter-reader variability". In: *European Journal of Radiology* 135 (2021), p. 109514.
- [3] Lars Heiliger et al. "Beyond Medical Imaging-A Review of Multimodal Deep Learning in Radiology". In: (2022).
- [4] P Kalavathi and VB Prasath. "Methods on skull stripping of MRI head scan images—a review". In: *Journal of digital imaging* 29.3 (2016), pp. 365–379.
- [5] Snehashis Roy et al. "Robust skull stripping using multiple MR image contrasts insensitive to pathology". In: *Neuroimage* 146 (2017), pp. 132–147.
- [6] Siddhesh P Thakur et al. "Skull-stripping of glioblastoma MRI scans using 3D deep learning". In: *International MICCAI Brainlesion Workshop*. Springer. 2019, pp. 57–68.
- [7] Arno Klein et al. "Evaluation of 14 nonlinear deformation algorithms applied to human brain MRI registration". In: *Neuroimage* 46.3 (2009), pp. 786–802.
- [8] Zeynettin Akkus et al. "Deep learning for brain MRI segmentation: state of the art and future directions". In: *Journal of digital imaging* 30.4 (2017), pp. 449–459.
- [9] Bjoern H Menze et al. "The multimodal brain tumor image segmentation benchmark (BRATS)". In: *IEEE transactions on medical imaging* 34.10 (2014), pp. 1993–2024.
- [10] Hendrik Mattern et al. "Chemical shift-based prospective k-space anonymization". In: *Magnetic resonance in medicine* 85.2 (2021), pp. 962–969.
- [11] Ana Morais, Jan Egger, and Victor Alves. "Automated computer-aided design of cranial implants using a deep volumetric convolutional denoising autoencoder". In: *World Conference on Information Systems and Technologies*. Springer. 2019, pp. 151–160.
- [12] Roberto Souza et al. "An open, multi-vendor, multi-field-strength brain MR dataset and analysis of publicly available skull stripping methods agreement". In: *NeuroImage* 170 (2018), pp. 482–494.
- [13] Li-Ming Hsu et al. "Automatic Skull stripping of rat and mouse brain MRI data using U-net". In: *Frontiers in neuroscience* 14 (2020), p. 935.
- [14] Riccardo De Feo et al. "Automated joint skull-stripping and segmentation with Multi-Task U-Net in large mouse brain MRI databases". In: *NeuroImage* 229 (2021), p. 117734.
- [15] Michele Avanzo et al. "Machine and deep learning methods for radiomics". In: *Medical physics* 47.5 (2020), e185–e202.
- [16] Cynthia B Paschal and H Douglas Morris. "K-space in the clinic". In: *Journal of Magnetic Resonance Imaging: An Official Journal of the International Society for Magnetic Resonance in Medicine* 19.2 (2004), pp. 145–159.
- [17] Philippe Lambin et al. "Radiomics: extracting more information from medical images using advanced feature analysis". In: *European journal of cancer* 48.4 (2012), pp. 441–446.
- [18] Kathrin Tingelhoff et al. "Analysis of manual segmentation in paranasal CT images". In: *European archives of oto-rhino-laryngology* 265.9 (2008), pp. 1061–1070.
- [19] P Kalavathi and VB Prasath. "Methods on skull stripping of MRI head scan images—a review". In: *Journal of digital imaging* 29.3 (2016), pp. 365–379.
- [20] Marijn E Brummer et al. "Automatic detection of brain contours in MRI data sets". In: *IEEE Transactions on medical imaging* 12.2 (1993), pp. 153–166.
- [21] Benoit M Dawant et al. "Automatic 3-D segmentation of internal structures of the head in MR images using a combination of similarity and free-form transformations. I. Methodology and validation on normal subjects". In: *IEEE transactions on medical imaging* 18.10 (1999), pp. 909–916.
- [22] Zu Y Shan, Guang H Yue, and Jing Z Liu. "Automated histogram-based brain segmentation in T1-weighted three-dimensional magnetic resonance head images". In: *NeuroImage* 17.3 (2002), pp. 1587–1598.
- [23] Stephen M Smith. "Fast robust automated brain extraction". In: *Human brain mapping* 17.3 (2002), pp. 143–155.
- [24] Yaping Wang et al. "Robust deformable-surface-based skull-stripping for large-scale studies". In: *International Conference on Medical Image Computing and Computer-Assisted Intervention*. Springer. 2011, pp. 635–642.
- [25] Simon F Eskildsen et al. "BEaST: brain extraction based on nonlocal segmentation technique". In: *NeuroImage* 59.3 (2012), pp. 2362–2373.
- [26] Florent Ségonne et al. "A hybrid approach to the skull stripping problem in MRI". In: *Neuroimage* 22.3 (2004), pp. 1060–1075.
- [27] Horst K Hahn and Heinz-Otto Peitgen. "The skull stripping problem in MRI solved by a single 3D watershed transform". In: *International Conference on medical image computing and computer-assisted intervention*. Springer. 2000, pp. 134–143.
- [28] Anders M Dale, Bruce Fischl, and Martin I Sereno. "Cortical surface-based analysis: I. Segmentation and surface reconstruction". In: *Neuroimage* 9.2 (1999), pp. 179–194.
- [29] Jan Egger et al. "Deep learning—a first meta-survey of selected reviews across scientific disciplines, their commonalities, challenges and research impact". In: *PeerJ Computer Science* 7 (2021), e773.
- [30] Jan Egger et al. "Medical deep learning—A systematic meta-review". In: *Computer Methods and Programs in Biomedicine* 221 (2022), p. 106874. ISSN: 0169-2607. DOI: <https://doi.org/10.1016/j.cmpb.2022.106874>. URL: <https://www.sciencedirect.com/science/article/pii/S0169260722002565>.

- [31] Jens Kleesiek et al. "Deep MRI brain extraction: A 3D convolutional neural network for skull stripping". In: *NeuroImage* 129 (2016), pp. 460–469.
- [32] Fabian Isensee et al. "Automated brain extraction of multisequence MRI using artificial neural networks". In: *Human brain mapping* 40.17 (2019), pp. 4952–4964.
- [33] Joshua Bassey, Lijun Qian, and Xianfang Li. "A survey of complex-valued neural networks". In: *arXiv preprint arXiv:2101.12249* (2021).
- [34] Shangshang Shi et al. "Quantum-inspired complex convolutional neural networks". In: *Applied Intelligence* (2022), pp. 1–10.
- [35] Yoseo Han, Leonard Sunwoo, and Jong Chul Ye. " $\{k\}$ -space deep learning for accelerated MRI". In: *IEEE transactions on medical imaging* 39.2 (2019), pp. 377–386.
- [36] Feng Huang, Wei Lin, and Yu Li. "Partial fourier reconstruction through data fitting and convolution in k-space". In: *Magnetic Resonance in Medicine: An Official Journal of the International Society for Magnetic Resonance in Medicine* 62.5 (2009), pp. 1261–1269.
- [37] Qiaoying Huang et al. "Brain segmentation from k-space with end-to-end recurrent attention network". In: *International Conference on Medical Image Computing and Computer-Assisted Intervention*. Springer. 2019, pp. 275–283.
- [38] Zhenmou Yuan et al. "SARA-GAN: Self-attention and relative average discriminator based generative adversarial networks for fast compressed sensing MRI reconstruction". In: *Frontiers in Neuroinformatics* (2020), p. 58.
- [39] Ian Goodfellow et al. "Generative adversarial nets". In: *Advances in neural information processing systems* 27 (2014).
- [40] Erik Bresch and Shrikanth Narayanan. "Region segmentation in the frequency domain applied to upper airway real-time magnetic resonance images". In: *IEEE transactions on medical imaging* 28.3 (2008), pp. 323–338.
- [41] Olaf Ronneberger, Philipp Fischer, and Thomas Brox. "U-net: Convolutional networks for biomedical image segmentation". In: *International Conference on Medical image computing and computer-assisted intervention*. Springer. 2015, pp. 234–241.
- [42] Ronald Newbold Bracewell and Ronald N Bracewell. *The Fourier transform and its applications*. Vol. 31999. McGraw-hill New York, 1986.
- [43] William T Cochran et al. "What is the fast Fourier transform?" In: *Proceedings of the IEEE* 55.10 (1967), pp. 1664–1674.
- [44] Michael Mathieu, Mikael Henaff, and Yann LeCun. "Fast training of convolutional networks through ffts". In: *arXiv preprint arXiv:1312.5851* (2013).
- [45] Harry Pratt et al. "Fcn: Fourier convolutional neural networks". In: *Joint European Conference on Machine Learning and Knowledge Discovery in Databases*. Springer. 2017, pp. 786–798.
- [46] Ronald Newbold Bracewell and Ronald N Bracewell. *The Fourier transform and its applications*. Vol. 31999. McGraw-hill New York, 1986.
- [47] David T Wymer et al. "Phase-contrast MRI: physics, techniques, and clinical applications". In: *Radiographics* 40.1 (2020), pp. 122–140.
- [48] Sofia Chavez, Qing-San Xiang, and Li An. "Understanding phase maps in MRI: a new outline phase unwrapping method". In: *IEEE transactions on medical imaging* 21.8 (2002), pp. 966–977.
- [49] Donald W McRobbie et al. *MRI from Picture to Proton*. Cambridge university press, 2017.
- [50] Jan Egger et al. "GBM volumetry using the 3D Slicer medical image computing platform". In: *Scientific reports* 3.1 (2013), pp. 1–7.
- [51] Florian Knoll et al. "fastMRI: A publicly available raw k-space and DICOM dataset of knee images for accelerated MR image reconstruction using machine learning". In: *Radiology: Artificial Intelligence* 2.1 (2020), e190007.
- [52] Jure Zbontar et al. "fastMRI: An open dataset and benchmarks for accelerated MRI". In: *arXiv preprint arXiv:1811.08839* (2018).
- [53] Adam Paszke et al. "PyTorch: An Imperative Style, High-Performance Deep Learning Library". In: *Advances in Neural Information Processing Systems* 32. Ed. by H. Wallach et al. Curran Associates, Inc., 2019, pp. 8024–8035. URL: <http://papers.neurips.cc/paper/9015-pytorch-an-imperative-style-high-performance-deep-learning-library.pdf>.
- [54] Elizabeth K Cole et al. "Analysis of deep complex-valued convolutional neural networks for MRI reconstruction". In: *arXiv preprint arXiv:2004.01738* (2020).
- [55] Mohamed Trabelsi, Panagiotis Kakosimos, and Hasan Komurcugil. "Mitigation of grid voltage disturbances using quasi-Z-source based dynamic voltage restorer". In: *2018 IEEE 12th International Conference on Compatibility, Power Electronics and Power Engineering (CPE-POWERENG 2018)*. IEEE. 2018, pp. 1–6.
- [56] Sergey Ioffe and Christian Szegedy. "Batch normalization: Accelerating deep network training by reducing internal covariate shift". In: *International conference on machine learning*. PMLR. 2015, pp. 448–456.
- [57] Oren Rippel, Jasper Snoek, and Ryan P Adams. "Spectral representations for convolutional neural networks". In: *Advances in neural information processing systems* 28 (2015).
- [58] Michal Drozdal et al. "The importance of skip connections in biomedical image segmentation". In: *Deep learning and data labeling for medical applications*. Springer, 2016, pp. 179–187.
- [59] Diederik P Kingma and Jimmy Ba. "Adam: A method for stochastic optimization". In: *arXiv preprint arXiv:1412.6980* (2014).

- [60] Lee R Dice. “Measures of the amount of ecologic association between species”. In: *Ecology* 26.3 (1945), pp. 297–302.
- [61] Abdel Aziz Taha and Allan Hanbury. “An efficient algorithm for calculating the exact Hausdorff distance”. In: *IEEE transactions on pattern analysis and machine intelligence* 37.11 (2015), pp. 2153–2163.